

Tracking with UAV using Tangent-plus-Lyapunov Vector Field Guidance

Hongda Chen and KuoChu Chang

Dept. of Systems Engineering and Operations Research
 George Mason University
 Fairfax, VA, U.S.A.
 {hchend, [kchang](mailto:kchang@gmu.edu)}@gmu.edu

Craig S. Agate

Algorithms R&D
 Toyon Research Corporation
 Goleta, CA, U.S.A.
 cagate@toyon.com

Abstract - A dynamic path-planning algorithm is proposed for routing UAVs in order to track ground targets. Based on a combination of tangent vector field guidance (TVFG) and Lyapunov vector field guidance (LVFG), a theoretically optimal path is derived with UAV operational constraints given a target position and the current UAV dynamic state. In this paper, we first illustrate that path planning for a UAV tracking a ground target can be formulated as an optimal control problem consisting of a system dynamic, a set of boundary conditions, control constraints and a cost criterion. We then discuss the TVFG and LVFG, and demonstrate that the TVFG outperforms the LVFG as long as a tangent line is available between the UAV's turning limit circle and an objective circle, which is a desired orbit pattern over a target. Particle filters are employed in a practical situation where a target is moving on a road network. Obstacle avoidance strategies are also addressed. With the help of computer simulations, we show that the T+LVFG algorithm provides effective and robust tracking performance in various scenarios, including a target moving according to waypoints or a random kinematics model in an environment that may include obstacles and/or wind.

Keywords: UAV, Target tracking, Path-planning algorithm, Particle filters, Obstacle avoidance, TVFG and LVFG.

1 Problem Description

Path planning for multiple UAVs to cooperatively track ground targets is an important research topic with approaches varying from classical optimal trajectory planning to bio-inspired swarm behavior [1], [2], [3]. In this paper we formulate the path planning algorithm for a UAV tracking a ground target as an optimal control problem consisting of a system dynamic, a set of boundary conditions, control constraints, and a cost criterion [4], [5], [6]. The equation $\dot{x} = f(t, x, u)$ describes the time-evolution of the UAV dynamic state $x = [x_1, x_2, \dots, x_n]$, which depends on the control input $u = [u_1, u_2, \dots, u_m]$. A cost function for evaluating a particular UAV trajectory

often contains at least one term of measure describing the distance between the final UAV state and the desired UAV state. In general, the optimal control problem can be formulated as

$$\begin{aligned} \min \quad & [x(t_2) - x_*]^2 + \int_{t_1}^{t_2} h[t, x(t), u(t)] dt \\ \text{s.t.} \quad & \dot{x}(t) = f[t, x(t), u(t)] \\ & x(t) \in X; u(t) \subseteq \Omega \end{aligned} \quad (1)$$

where x_* is the desired UAV state, and X, Ω are the UAV state and control space, respectively. The second term in the objective function is the cost of the UAV state trajectory along the path from $x(t_1)$ to $x(t_2)$. The cost objective in (1) is to be minimized in order to produce the optimal control solution. However, the overall costs will be UAV dependent and could include factors such as power (battery, gas) consumption, communication, mission scheduling with multiple UAVs and so on. Based on the assumption that each UAV has the capability to complete the tracking assignment, the cost function is dramatically simplified. In this paper, the only physical limitations we considered are a UAV's maximum turn rate and a nominal cruising speed. Consequently, the simplified objective is just the distance measurement.

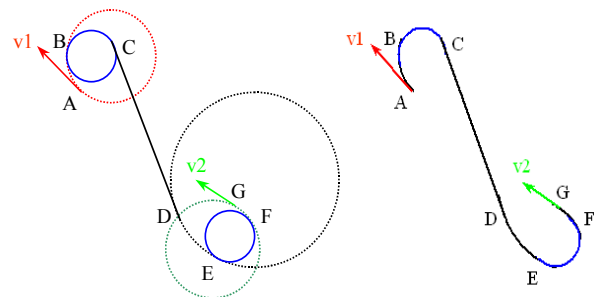


Figure 1. UAV path planning (L) and selected path (R).

In the left diagram of Figure 1, UAV starts at point 'A' with initial velocity v_1 , and ends at desired endpoint 'G' with velocity v_2 . The optimal path (minimal traveling distance) follows $A \rightarrow B \rightarrow C \rightarrow D \rightarrow E \rightarrow F \rightarrow G$ in which the blue circles correspond to minimal turn radius, the black circle corresponds to maximal velocity, the red circle corresponds to the current velocity, and the green circle corresponds to the final velocity. The optimal path from A

to G can be illustrated as in the right side of Figure 1. Therefore, the optimal control problem can be described as: given UAV position and velocity at points A and G, find the points B/C/D/E/F such that the cost function is minimized. In the subsequent section, we will show that the shortest path is found using what we shall call tangent vector guidance.

The dynamic path-planning algorithm requires the following information about the system state: (i) the predicted target state; (ii) the current UAV state; and (iii) the *desired* UAV state. In practice, the UAV state at any time step is known, and the target state is estimated from collected sensor data. The desired UAV state is given by the following conditions: (i) the UAV is positioned on a circle of fixed radius about the estimated target location; (ii) the UAV's heading is equal to the target's heading; and (iii) the UAV's speed is equal to the target's speed unless the target speed is less than the UAV's minimal speed in which case the UAV's speed is set to its minimum. The UAV's desired state is therefore dependent on the target state and can be determined through different approaches (e.g., a desired position may be chosen to maximize the probability of detecting the target at some future time). The UAV vehicle control includes a set of possible choices, such as: turn left, turn right, ascend, descend, or go straight.

2 UAV Flight Guidance

2.1 Lyapunov vector field guidance

Using a Lyapunov vector field guidance law (LVFG) [7], the guidance of a UAV to an observation 'orbit' around a target can be determined by building a vector field that has a stable limit cycle centered on the target position. The UAV is assumed to be able to move freely but only in the direction of its orientation. As defined in [8], the UAV dynamics can be modeled as

$$\dot{x} = V \cdot \cos \theta; \quad \dot{y} = V \cdot \sin \theta; \quad \dot{\theta} = w \quad (2)$$

where the inputs v, w denote lateral and angular velocity, whose constraints are given by $v_{\min} \leq V \leq v_{\max}$ and $-\alpha \leq w \leq \alpha$. A UAV traveling at constant speed without slipping will experience a minimum turning radius so that the angular velocity is bounded by $|w| \leq V / R$. Assume $[x, y]^T$ is the two-dimensional inertial position of the aircraft, and $p = [x_r, y_r]^T$ is the position of the aircraft relative to the target. A Lyapunov vector field law can be used to determine the guidance of a UAV by calculating the desired velocity. Consider the Lyapunov function $\Gamma(p) = (r^2 - R_t^2)^2$ in which $r = \sqrt{x_r^2 + y_r^2}$ is the radial distance of the UAV from the target and R_t is the radius of the stand-off circle. The total time derivative of $\Gamma(p)$ can be specified to be non-positive by choosing a desired relative vehicle velocity according to the guidance vector field, such that [7],

$$\begin{bmatrix} \dot{x}_d \\ \dot{y}_d \end{bmatrix} = -\lambda \begin{bmatrix} r^2 - R_t^2 & 2rR_t \\ -2rR_t & r^2 - R_t^2 \end{bmatrix} \begin{bmatrix} x_r \\ y_r \end{bmatrix} \quad (3)$$

in an anti-clockwise direction, or

$$\begin{bmatrix} \dot{x}_d \\ \dot{y}_d \end{bmatrix} = -\lambda \begin{bmatrix} r^2 - R_t^2 & -2rR_t \\ 2rR_t & r^2 - R_t^2 \end{bmatrix} \begin{bmatrix} x_r \\ y_r \end{bmatrix} \quad (4)$$

in a clockwise direction, where λ is a non-negative normalization factor.

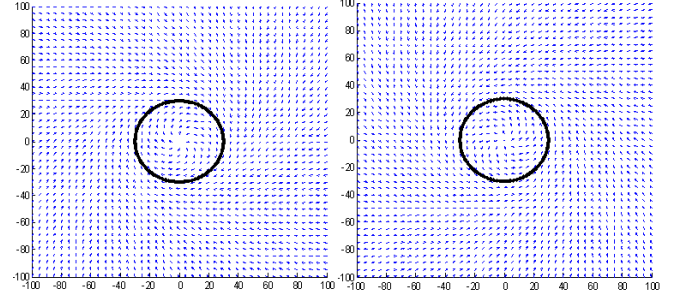


Figure 2. Clockwise/anti-clock LVFG with $R_t = 30m$.

With (3) and (4), the vector field vectors produce a non-positive rate of change of $\Gamma(\cdot)$. If λ is bounded away from zero, $\Gamma(\cdot)$ is zero and invariant only on the stand-off circle ($r = R_t$), it ensures [7] that the vector field produces a globally attractive limit cycle.

Figure 2 illustrates the guidance vectors surrounding a stationary target in anti-clockwise and clockwise orientations, respectively. It is clear that a path following the field vectors from any point will end up on a circle of radius equal to the specified stand-off distance (shown in black).

2.2 Tangent vector field guidance

In [8], we proposed a dynamic path-planning algorithm for a UAV that is tracking a ground target. A theoretically optimal path was derived with UAV operational constraints given a target position and the current UAV kinematic state. Since the desired direction is always following the tangent line to the stand-off circle, we refer to the path planning approach as the tangent vector field guidance (TVFG) law. The limitation of TVFG is that the UAV must be outside the stand-off circle; otherwise, a tangent line does not exist and the TVFG cannot provide a proper guidance. In that case, the proposed strategy in [8] simply moves the UAV forward based on its current speed (once the UAV is outside the stand-off circle, the TVFG can, once again, be used).

In general, for any 2D point, (x_u, y_u) , outside of an objective circle with radius R_c and center (x_c, y_c) , we can easily calculate two tangent points on the circle, such that

$$\begin{cases} x_{1,2} = \frac{R_c^2}{r_u^2}(x_u - x_c) \mp \frac{R_c}{r_u^2}(y_u - y_c)\sqrt{r_u^2 - R_c^2} + x_c \\ y_{1,2} = \frac{R_c^2}{r_u^2}(y_u - y_c) \pm \frac{R_c}{r_u^2}(x_u - x_c)\sqrt{r_u^2 - R_c^2} + y_c \end{cases} \quad (5)$$

where $r_u = \sqrt{(x_u - x_c)^2 + (y_u - y_c)^2}$. In that case, assuming $[x_o, y_o]^T$ is the tangent point on the standoff circle, the UAV direction angle can be determined as

$$\phi_r = \arctan \left[\frac{y_u - y_o}{x_u - x_o} \right] \quad (6)$$

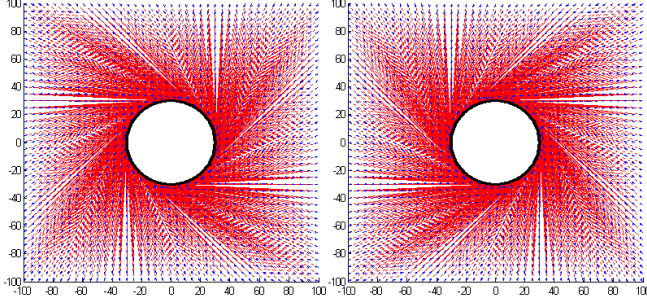


Figure 3. Clockwise/anti-clock TVFG with $R_t = 30m$.

The desired relative vehicle velocity according to the guidance vector field is

$$\begin{bmatrix} \dot{x}_d \\ \dot{y}_d \end{bmatrix} = \lambda_2 \cdot \begin{bmatrix} \cos \phi_r \\ \sin \phi_r \end{bmatrix} \quad (7)$$

Figure 3 visualizes the TVFG vectors surrounding a stationary target with clockwise and anti-clockwise orientations, respectively. It is clear that a path following the field vectors from any point will end up on a circle of radius equal to the specified standoff distance (shown in black). Moreover, it is easy to show the following results:

Proposition 1. *In the sense of shortest distance for a UAV going to an objective circle around a target, whenever TVFG is available, the optimal UAV path is found using the nearest TVFG.*

Proposition 2. *As long as the tangent lines are available between a UAV's turning limit circle and an objective circle, TVFG provides more efficient (in the sense of shortest path) path planning than LVFG.*

Proposition 2 can be directly derived from Proposition 1. Here we omit the proofs. However, in order to compare the performance of the two guidance laws, when any tangent lines are available, we introduce distance and time efficiency measures to evaluate the UAV path planning efficiency. In Figure 4, we present a coordinate diagram with UAV, target, and wind, where the red circle is the objective trajectory around the target. The distance between UAV and target is denoted as “d”. The relative UAV heading direction to the target, is denoted ρ , and α is the

relative direction of *Wind*. The distance and time efficiency are then defined as D_x / d and $T_x \bar{V} / d$, respectively. Here D_x denotes the UAV total flight distance to the objective circle, and T_x is the total time used to travel to the objective circle. \bar{V} is the average speed of UAV. Notice that in the case of a UAV with constant speed, the time efficiency and distance efficiency are equivalent.

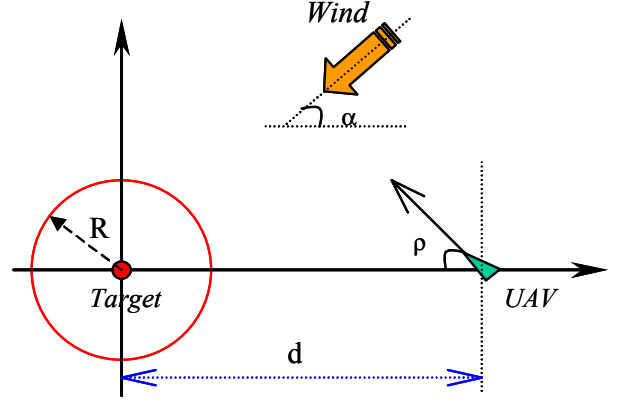


Figure 4. Illustration diagram with UAV, target and wind.

Figure 5 plots two example trajectories when $\rho = 0$ and $\rho = \pi$, respectively. The UAV speed is constant at 14 m/s, the turning limit is $\pi/6$, and the sampling period is 1s. The objective circle is 30m, target is located at (0,0) and the initial UAV is at (100m,100m). When the LVFG provides a non-feasible direction due to the current UAV kinematic limit, we simply apply the maximum turning rate as in the TVFG. For example, the first four initial states from the two strategies are the same as shown in the right of the Figure 4. Note that in general TVFG provides more efficient waypoints to reach the objective orbit. Additionally, we observe that the LVFG cannot precisely reach the desired orbit. The offsets depend on UAV's velocity and sampling interval.

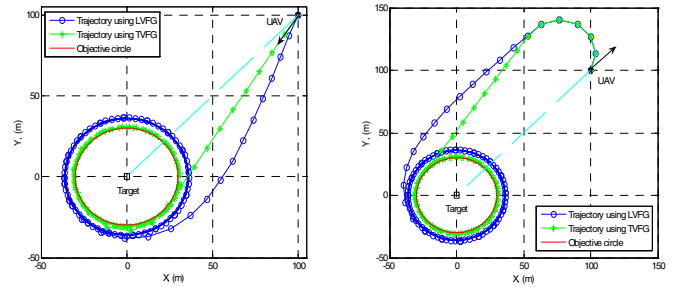


Figure 5. Examples of UAV paths with different UAV initial heading angles.

Figure 6 plots the distance/time efficiency as a function of relative angle between 0 to π . Here, in order to have a fair comparison, we use the LVFG's orbit as the objective for evaluation. Time and distance efficiency are identical since we assume that UAV's speed is constant. Notice that the TVFG performs about 40% better than the LVFG.

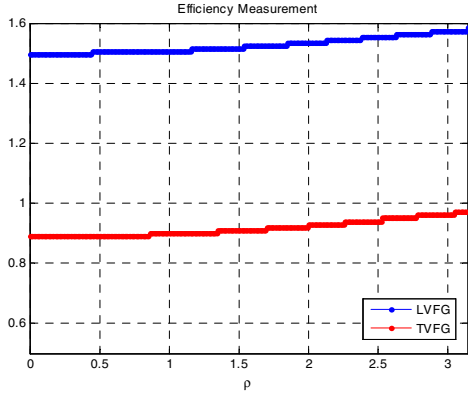


Figure 6. Efficiency Performance of LVFG and TVFG.

Unfortunately, there is no tangent line to the objective circle when we start from a point within the circle. Thus, we can either simply move the UAV forward based on its current speed since the target is in the UAV's field of view (FOV) anyway, or use another simple strategy to provide a complete guidance.

2.3 T+L vector field guidance (T+LVFG)

Here, we propose a hybrid strategy to combine TVFG and LVFG, such that whenever UAV is outside the standoff circle, we use TVFG, and whenever UAV is inside the standoff circle, we use LVFG. We refer to this hybrid strategy as the T+LVFG algorithm. Results show that whenever TVFG is available, it provides more efficient, effective and robust performance to track a target than LVFG. Additionally, we noted that LVFG alone has a much larger bias to a given objective circle.

As the UAV tracks a target along a standoff circle, the average distance between the UAV trajectory and the standoff circle in steady-state is defined as the average steady-state bias (ASB). Since the guidance law when the UAV is within the circle is the same for the T+LVFG and LVFG alone, we consider the ASB for the T+LVFG and LVFG alone only when the UAV starts outside the objective circle and attempts to approach and fly along the objective circle. Once the UAV reaches the objective circle it attempts to fly along the objective circle. Due to the finite sampling rate, the UAV cannot fly along the circle exactly but reaches a steady state with an error between the objective circle and the UAV's actual flight path. In general, we have the following result:

Proposition 3. Suppose that a UAV has a speed V and a sampling time Δ . In the case of its tracking a stationary target along a standoff circle R_c , the T+LVFG provides much smaller ASB than the LVFG alone, such that

(i) In T+LVFG, ASB is bounded by

$$\sqrt{R_c^2 + \frac{1}{4}V^2\Delta^2} - R_c;$$

(ii) In LVFG alone, ASB is given by

$$\sqrt[3]{-q + \sqrt{q^2 + p^3}} + \sqrt[3]{-q - \sqrt{q^2 + p^3}} + \frac{1}{6}V\Delta - R_c,$$

where $q = -\frac{1}{216}V^3\Delta^3 - \frac{1}{3}V\Delta R_c^2$ and $p = -\frac{1}{36}V^2\Delta^2 - \frac{1}{3}R_c^2$.

The proof of Proposition 3 is straightforward, and omitted here. Figure 7 plots the ASBs with different sampling intervals and a UAV speed of 14m/s. At the objective circle of 40m with one second sampling time, we observe that the bias is 0.65m and 6.5m for the T+LVFG and the LVFG, respectively.

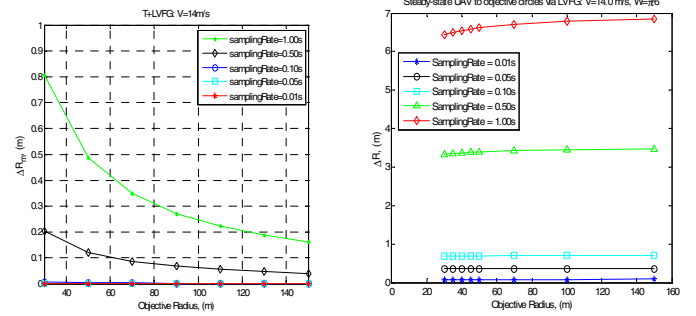


Figure 7. Plot of ASB versus objective circle radius and sampling interval for the T+LVFG and LVFG approaches.

2.4 UAV control with winds

In the presence of a wind field, when expressed relative to a moving target $[x_t, y_t]^T$ with velocity $[\dot{x}_t, \dot{y}_t]^T$, the UAV model may be expressed as

$$\dot{x}_r = V \cdot \cos \theta + W_x - \dot{x}_t \quad (9)$$

$$\dot{y}_r = V \cdot \sin \theta + W_y - \dot{y}_t \quad (10)$$

where W_x and W_y are the components of the background (horizontal and vertical) wind velocity. Using the wind compensations in (9) and (10), LVFG and T+LVFG can both be applied to determine the guidance of UAV.

3 Target Motion Estimation and Maximizing Target Detection

As discussed previously, we base the UAV's desired location on the estimated location of the target. Choosing a target location estimate, such as the *expected* location, may be straightforward when the predicted target location probability density function (PDF) is uni-modal (e.g., Gaussian). However, in many practical ground target tracking scenarios, the ground vehicles move through a road network, which, due to the presence of road intersections, often results in predicted target PDFs that are multi-modal. By choosing a location that is close to the expected location of the target, we are essentially trying to improve the tracking picture through appropriate routing [9]. Under such circumstances we need a target state PDF representation that can represent multi-modal densities. Moreover, we need a basis for choosing the desired UAV location since using the expected target location for a multi-modal density may yield a location that is nowhere near the target. Thus, we use a point-mass approximation of the target state PDF and use stochastic simulation to propagate the PDF using a ground vehicle motion model that exploits road network

information (alternative approaches use target occupancy maps that define a piece-wise constant probability mass function over a grid, e.g., [10]). Once we generate a predicted target state PDF, we determine an “optimal” UAV location that maximizes the probability of detecting the target. Once we determine this desired UAV position, we generate the optimal UAV trajectory using the algorithm discussed previously.

3.1 Coverage in 2D space

We first discuss the coverage probabilities of a UAV and target in a 2D space. This simplified case assumes that the UAV and target can move along any directions without physical limitations. Figure 8 shows an example in which the UAV and target can move in any direction at any time instance. In the figure, the UAV is located at point “o”, and the tracked target is at point “g”.

With two time instances, the orange and light-blue circles represent the initial and subsequent (i.e., at the next time instance) FOVs of the UAV, respectively. The light-green circle represents the initial target location uncertainty assuming the target is currently located at “g”. Similarly, when target moves to “q”, the purple circle represents the predicted target location uncertainty at the next time instance. The light brown circle area represents corresponding potential UAV positions as it moves from the position “o”. Assuming uniform distributions (equally likely to move to all reachable positions) for both UAV and target, then at the initial time, the coverage probability is one since the orange circle covers the light-green circle completely. In other words, the target is fully covered by the UAV if the UAV does not move. However, at the next time step, the UAV has moved to point “p” and the target has moved to point “q”. The coverage probability is then defined as the fraction of the purple circle that is covered by the light-blue circle.

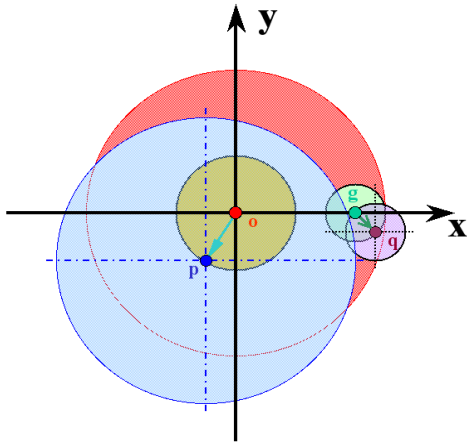


Figure 8. UAV coverage in two sequential time intervals.

More specifically, suppose the UAV position is (m'_u, n'_u) , and the target position is (m'_t, n'_t) . The heading directions

are assumed to be α and β , respectively. Then, at the next time step, the UAV and target positions can be expressed as

$$\begin{aligned} m_u &= m'_u + \Delta V_u \cos \alpha \\ n_u &= n'_u + \Delta V_u \sin \alpha \end{aligned} \quad (11)$$

$$\begin{aligned} m_t &= m'_t + \Delta V_t \cos \beta \\ n_t &= n'_t + \Delta V_t \sin \beta \end{aligned} \quad (12)$$

The radius of the UAV's coverage is assumed to be R_c , and target uncertainty radius (say, 3-sigma boundary) is R_t . The intersection points of the two circles may be found from the solutions of the following equations,

$$\begin{cases} (x - m_u)^2 + (y - n_u)^2 = R_c^2 \\ (x - m_t)^2 + (y - n_t)^2 = R_t^2 \end{cases} \quad (13)$$

Obviously, in the case of no real solution from (13), the coverage probability is either one or zero, which depends on the distance between UAV and the target, namely

$$d_0 = \sqrt{(m_t - m_u)^2 + (n_t - n_u)^2} \quad (14)$$

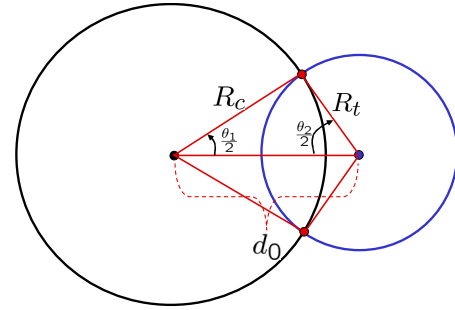


Figure 9 Geometry Illustration for two Angle Calculations.

If $d_0 \geq R_c + R_t$, the target is out of the FOV of the UAV so that the coverage probability is zero. If $d_0 \leq R_c - R_t$, the target is completely in the FOV of the UAV so that the coverage probability is one. Otherwise, in the geometrical sense, angles θ_1 and θ_2 in Figure 9 can be calculated by

the law of cosines, such that $\theta_1 = 2 \cos^{-1} \left(\frac{R_c^2 + d_0^2 - R_t^2}{2R_c d_0} \right)$

and $\theta_2 = 2 \cos^{-1} \left(\frac{R_t^2 + d_0^2 - R_c^2}{2R_t d_0} \right)$. Therefore, based on the

determined angles, one can readily show the following result.

Proposition 4. Suppose that the UAV's coverage radius is R_c and target uncertainty radius is R_t . The coverage probabilities can be expressed as

(i) In case of $R_c \geq R_t$, we have

$$\Pr = \begin{cases} \frac{s_1}{\pi R_t^2}, & \text{if } d_0 \geq \sqrt{R_c^2 - R_t^2} \\ 1 - \frac{s_2}{\pi R_t^2}, & \text{otherwise} \end{cases} \quad (15)$$

(ii) In case of $R_c < R_t$, we have

$$\Pr = \begin{cases} \frac{s_1}{\pi R_t^2}, & \text{if } d_0 \geq \sqrt{R_t^2 - R_c^2} \\ \frac{R_c^2}{R_t^2} + \frac{s_2}{\pi R_t^2}, & \text{otherwise} \end{cases} \quad (16)$$

where $s_1 \equiv \frac{1}{2}[\theta_2 - \sin(\theta_2)]R_t^2 + \frac{1}{2}[\theta_1 - \sin(\theta_1)]R_c^2$ and $s_2 \equiv \frac{1}{2}[\theta_2 - \sin(\theta_2)]R_t^2 - \frac{1}{2}[\theta_1 - \sin(\theta_1)]R_c^2$.

3.2 General coverage probabilities

In practice, due to the road and/or turning angle limitations, a UAV or a target cannot move freely to anywhere in their reachable circles and, therefore, the circular representation of the target's location uncertainty is insufficient. Our objective for choosing a desired UAV location (an input to the path-planning algorithm) was to maximize the probability of detection. Since the target's state is not known with certainty, we cannot calculate the probability of detecting a target given a potential position for the UAV, but, instead, we calculate the expected probability of detection:

$$E[P_d] = \int_{\Omega_s} D(\mathbf{x}) p(\mathbf{x}) d\mathbf{x} \quad (17)$$

where Ω_s presents the sensor FOV, $p(\mathbf{x})$ is the probability density function (PDF) of the target state (which may include both position and velocity), $D(\mathbf{x})$ represents a function that maps the target state into a probability of detection (this function could take into account the distance from the point \mathbf{x} to the sensor so that resolution affects Pd, it could take into account whether there is obscuration between point \mathbf{x} and sensor, etc.).

Note that $p(\mathbf{x})$ is obtained by extrapolating the target's kinematic state based on the road network information. The idea is to use a digital road map to constrain the possible target locations. In practice, it could be very difficult to model the density precisely due to road uncertainties. However, given a digital road map, Monte Carlo samples (particles) can be generated to describe possible target states, which yields two benefits. First, stochastic simulation allows us to handle more realistic on-road motion models (e.g., slowing at curves, pausing at intersections). Second, with a point-mass representation of the predicted target state PDF the integration part of (17) can be approximated by counting number of particles in the respective areas. Of course, there is significant room for improvement in selecting a UAV's destination objectives via a reliable estimate of its coverage probabilities. For instance, when UAV loses its target, simply counting

particles, the resulting coverage rate is clearly biased and incorrect.

3.3 Coverage rate with particles

As mentioned in the previous section, we plan to use particles to simulate possible target locations at the next time step in order to obtain a UAV's desired location. To do so, it is assumed that: (i) the UAV has been given the initial state (position/velocity) information about the target of interest; (ii) digital road map information is available; and (iii) in a tracking stage, the UAV could observe the latest target state information with its own sensor.

In this paper, it is assumed that the initial target information is available from at least one of the resources (GMTI or otherwise). After the initialization, the UAV must track the target using only sensor data collected by the UAV's onboard sensor. If the UAV cannot acquire the target on its own after the initial assignment, then it is highly likely that it will never track the target. In that case, a separate initialization/re-assignment process is needed.

The initial PDF of a target state is generally given based on the assumption that the target is following the roads in a given map, and its velocities are uniformly distributed between maximal and minimal speed limits. Thus, particles will be randomly drawn from this PDF. These particles are used to predict the target state forward in time based on the road network.

3.3.1 Generate target-location particles

To predict target state forward, we generate random samples based on a given road map information. These samples are obtained using the maximal and minimal target speeds together with random numbers characterized by appropriate distributions. If not explicitly mentioned, a Gaussian distribution is used to generate normal i.i.d. samples with mean zero and a given variance that could be estimated from the historical data. At any road intersection, we assume equal probability for all possible forward directions. Since a target could possibly turn around, a U-turn probability is also introduced.

3.3.2 Select destination objective

The desired UAV destination objective is a reachable position for the UAV within a given planning cycle that maximizes the probability of detecting the target, which amounts to the UAV location such that the maximum number of particles is within the UAV's FOV. Euclidean distances can be used to compare the destination objectives. Specifically, assume that there are N particles $\{P_i(x, y)\}$, and M candidate objectives $\{C_j(x, y)\}$, we have

$$d_{p \rightarrow c}(i, j) = |P_i(x, y) - C_j(x, y)| \quad (18)$$

Based on the UAV's FOV radius, the coverage probabilities can then be estimated as a ratio of the number of particles inside the UAV's FOV over the total number of particles,

$$\Pr(j) = \frac{1}{N} \sum_i \delta_{[d_{p \rightarrow c}(i,j) \leq R_c]} \quad (19)$$

For each candidate objective, the distance from the UAV's current position is

$$d_{u \rightarrow c}(j) = |U(x, y) - C_j(x, y)| \quad (20)$$

To determine the most desirable UAV destination objective based on (18) and (19), we must sample the set of reachable UAV states in order to render the number of potential locations to consider into a finite number. To select the destination candidates, one simple idea is to define them uniformly in the UAV reachable region based on maximum and minimum UAV speeds.

4 Obstacle Avoidance

In the meantime, we will consider the following problem: *How to make a UAV track a target while avoiding obstacles (including no flight zones) at the same time?* The information about the existence of the obstacles is either known in advance (e.g., buildings), or acquired during flight (e.g., collision avoidance with other aircraft). In most real scenarios more than one obstacle might appear, so multiple obstacles are considered. To handle situations of obstacle avoidance, an obstacle avoidance algorithm is added to the path-planning cycle to guide the UAV to move around the obstacle. This combination results in a scheme that reacts to the changing and uncertain environment.

We assume that the UAV is capable of receiving obstacle information at any path-planning cycle, by either its own sensors or other resources. Without loss of generality, obstacles are modeled as circles determined by their center position and radius. Other shapes may be treated in a conservative manner by inscribing them in a larger circle, thereby permitting the obstacle avoidance problem to be formulated in terms of a simplified model of turning circles similar to the shortest-path algorithm we described earlier. The obstacle avoidance problem is then interpreted as the shortest-path selection among all possible paths. Specifically, we first determine the closest obstacle for the UAV to move around by using a straight line to link the UAV and the destination circle about the target. Then, we start from this obstacle to locate the next possible obstacle if any, between the target and current obstacle circle. By doing this forward search step-by-step, all the possible paths and corresponding distances will be calculated. Therefore, a practical solution with the shortest distance can be selected.

More specifically, suppose the UAV is located at (m'_u, n'_u) , and the target is located at (m'_t, n'_t) . The UAV and the target headings (angles) are assumed to be α and β ,

respectively. During the path-planning cycle, assume L obstacle circles (no flight zones) appear unexpectedly. These obstacle circle parameters are assumed to be available, i.e., center coordinates, $(m_o^{[i]}, n_o^{[i]})$, and radius,

$R_o^{[i]}$. For simplicity, the obstacle circles are assumed to be non-overlapping in this paper. The intersection points of the obstacle circles and the path-line between the UAV and the target may be found from the solutions of the following equations,

$$\begin{cases} (x - m_o^{[i]})^2 + (y - n_o^{[i]})^2 = R_o^{[i]2}, & i = 1, 2, \dots, L \\ \frac{y - y_t}{y_u - y_t} = \frac{x - x_t}{x_u - x_t} \end{cases} \quad (20)$$

If there is no real solution in (20) for an obstacle- i , it means that this obstacle will not affect the current path planning, and we may ignore it at this moment. Otherwise, based on the distance measurements between UAV and the intersection points, we can readily locate the closest obstacle, which is blocking the path (marked as the most effective obstacle), and initiate the obstacle avoidance algorithm to plan the UAV path around it.

In general, the UAV will take the shortest distance by following the line path connecting the start point and the target point. In the case that a most effective obstacle is located, the path-planning algorithm will follow a tangent line to this obstacle. There are three basic situations to be considered: (i) the most effective obstacle (MEO) is independent; (ii) the most effective obstacle is dependent; and (iii) without effective obstacle.

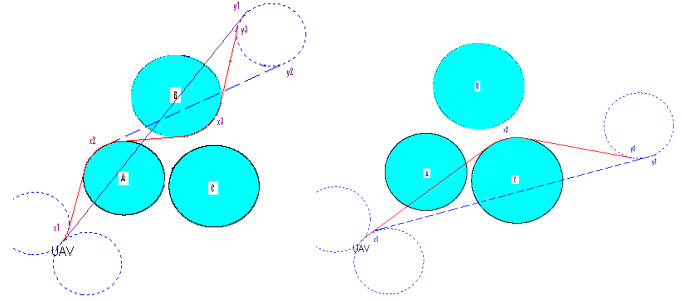


Figure 10 Two cases: (i) MEO independent, (ii) MEO dependent.

In the situation of without effective obstacles, path planning operates in normal condition, and obstacle avoidance algorithm is not needed to find the shortest path between the UAV and the target. As illustrated in Figure 10 (left), the path-line of "x1 → y1" crosses obstacle-A and obstacle-B, the first MEO can be identified as obstacle-A. The obstacle avoidance algorithm will select a path around obstacle-A first, such that "x1 → x2". Similarly, by the straight-line "x2 → y2", the subsequent MEO is identified as obstacle-B, and the obstacle avoidance algorithm will find a path to go around it. Therefore, the overall path could be obtained as "x1 → x2 → x3 → y3". The case of dependent MEO is illustrated in Figure 10 (right). As the path-line of "x1 → y1" crosses only obstacle-C, a MEO is identified as

obstacle-C. The obstacle avoidance algorithm will select a path around obstacle-C, e.g., “x1→x2”. However, this new path will cross another obstacle-A, which will affect the current path plan. Therefore, adjustments of the path plan need to be made first to avoid obstacle-A.

5 Numerical Results

Multiple simulation scenarios are provided in this section to illustrate the performance of the newly proposed dynamic UAV path-planning algorithm for ground target tracking. First, we consider three examples of different target-moving models [8]: (i) a target is moving with a kinematic model (nearly constant velocity) in 2D free space; (ii) a target is moving within time-based waypoints; (iii) a target is moving within speed-based waypoints. Then, we consider different wind environments to present its robustness for UAV tracking a stationary and/or moving target. After that, we present detection probabilities using an example. Moreover, particle filters will be employed in two different map considerations. Finally, the obstacle avoidance algorithm will be validated as multiple obstacles may appear in dynamic path generations.

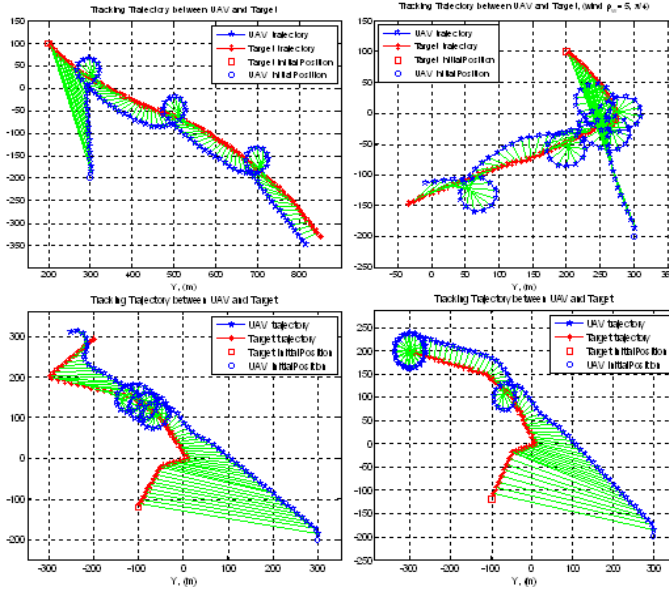


Figure 11. T+LVFG tracking performance in different cases.

In the first scenario, a UAV initial position is assumed at $[x_0 = 300, y_0 = -200]m$ and a height of $100m$. It has a nominal speed of $14m/s$ with a heading angle $[54$ degree (East is 0 degree)]. The UAV maximal turning rate is 30 degree per second. Both sampling rate and planning cycle are one second. Using T+LVFG, Figure 11 plots four cases as a target follows the kinematic model (upper two charts), speed-based waypoint model (lower left), and time-based waypoint model (lower right). In the upper left chart of the kinematic model, the initial target position is assumed as $[x'_0 = 200, y'_0 = 100]m$ with an initial speed of $5m/s$ at

heading angle -45 degree. The target maximal speed is $12m/s$, and the state process noise standard deviation is 0.1 . In addition, a constant wind of strength 5.0 and angle 45 degree is presented at the upper right chart. In the speed-based model, target is with a constant speed in each line space (road section). Specifically, in the moving segments of $[(x'_0, y'_0): (-100, -120)] \rightarrow [(x'_1, y'_1): (-50, -20)] \rightarrow [(x'_0, y'_0): (10, 0)] \rightarrow [(x'_1, y'_1): (-50, 102)] \rightarrow [(x'_1, y'_1): (-110, 150)] \rightarrow [(x'_1, y'_1): (-300, 200)]$, the target speeds are $10m/s, 8m/s, 7m/s, 2m/s, 15m/s, 12m/s,$ and $14m/s$, respectively. In the time-based model, the target arrives to these denoted points at time of $0s, 8s, 18s, 37s, 52s, 68s$ then stops at the final position. Results show that the T+LVFG algorithm provides an efficient and effective solution in those cases considered.

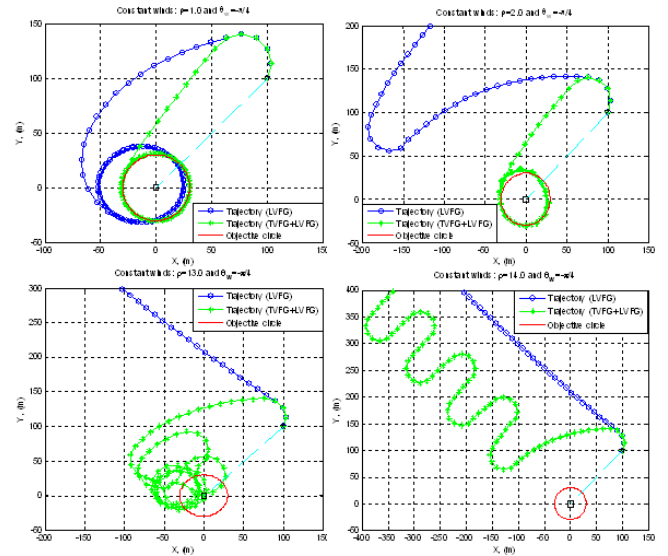


Figure 12. Performance comparisons within different winds.

To demonstrate the robustness under wind conditions of the T+LVFG algorithm, we now consider a case in which the UAV tracks a stationary target. Suppose that a UAV’s relative-angle to target is π , turn-limit is 30 degree per second and speed $14m/s$. Figure 12 plots the UAV and target trajectories in different wind environments. In the upper left, are the trajectories using LVFG and T+LVFG under a wind condition of $\rho_w = 1.0m/s$ and $\theta_w = -\frac{\pi}{4}$. While in this case the T+LVFG yields similar paths with or without the presence of wind, the LVFG alone has a big distortion and a shifted-orbit as we expect. In the upper right, the wind strength is increased to $\rho_w = 2.0m/s$ and the flowing angle is $-\pi/4$. Notice that while the T+LVFG algorithm has a slightly distorted path along the objective circle, the LVFG alone diverges in these mild wind considerations. As shown in the lower left-hand plot, at a high wind speed of $13.0m/s$, the T+LVFG algorithm struggles but manages to eventually get the target within the FOV, though the trajectory fails to accurately follow the objective circle. Unfortunately, when the wind speed is the

same or higher than UAV's speed, the UAV cannot compensate for the wind and, therefore, cannot reach the objective circle. An example result when the wind speed is the same as the UAV speed limit of 14m/s is shown in the lower right plot in which both algorithms diverge.

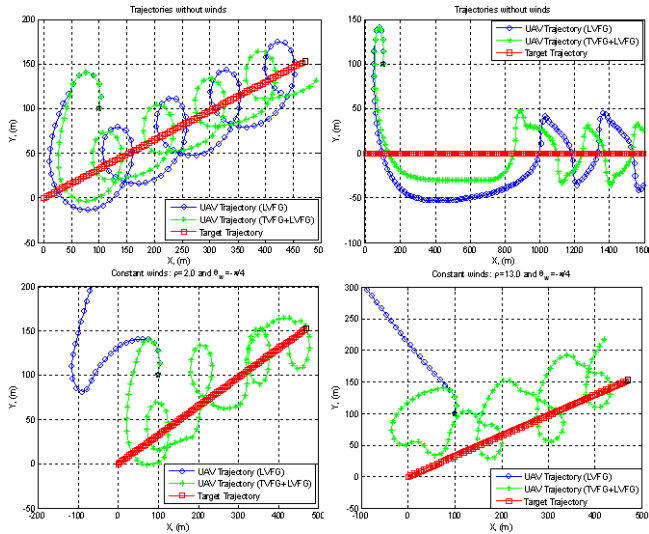


Figure 13. Performance comparisons for a moving target.

Next, we apply the newly proposed T+LVFG algorithm for a UAV that tracks a moving target under windy conditions. The UAV has the same parameters as in the case of tracking a stationary target. Figure 13 shows the tracking results for a moving target with and without winds. In the upper left, the moving target is with a constant velocity 5m/s, starts from (0,0), and moves along a direction angle of $\theta_t = \frac{\pi}{10}$. Since the UAV is much faster than the target, both algorithms demonstrate that the UAV's trajectories are screw lines along the target trajectory. However, the T+LVFG algorithm provides closer and more efficient tracks that the LVFG alone. In the upper right, a faster target, which has a constant velocity of 12m/s, is considered. The target starts from (0,0) and heads due east. Again the path corresponding to the T+LVFG algorithm is generally closer to the target. In the lower charts, winds with 2m/s and 13m/s are considered. The T+LVFG algorithm works well, but the LVFG alone fails in both cases.

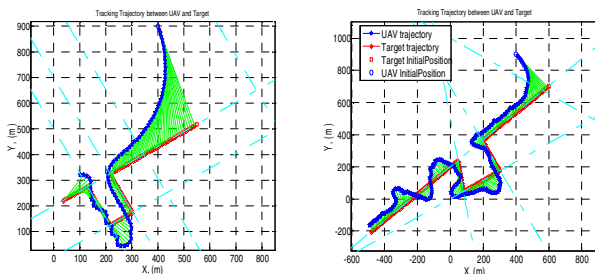


Figure 14. Tracking results using particle filters.

Figure 14 illustrates simulation results using a point-mass approximation of the target predicted PDF and choosing a desired UAV location based on maximizing the probability of detecting the target. The two plots show the corresponding tracking results via the particle filter strategy. In each planning step, we generate 100 particles for the predicted target location and select 50 destination candidates uniformly in the UAV's reachable region. At each planning cycle, we select the UAV destination based on maximizing the probability of detecting the target.

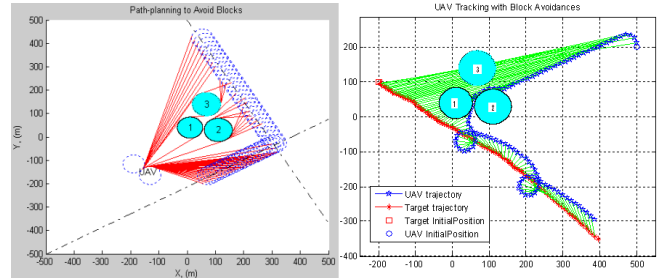


Figure 15. Path planning and tracking results using the obstacle avoidance strategy.

Finally, we evaluate the obstacle avoidance strategies in the dynamic path-planning algorithm. Suppose that there are three obstacles in a path-planning environment. The simulated obstacles are defined as Obstacle-1, centered at [10,40]m and radius is 45m, Obstacle-2, centered at [110,30]m and radius is 50m, and Obstacle-3, centered at [68,140]m and radius is 50m. In the left of Figure 15, the initial position of UAV is fixed at [-160,-140]m, and a heading of 50 degrees. A target is following a road map. The optimal paths are plotted with different target positions, and obstacles are successfully avoided. In the right of Figure 16, the same obstacles are presented. A target is moving with a kinematic model in 2D free space [8], the initial target position is assumed as $[x'_0 = -200, y'_0 = 100]m$ with an initial speed of 5m/s and heading of -45 degrees. The target maximal speed is 12m/s, and the state process noise standard deviation is 0.1. The UAV is initially located at [500,200]m with velocity [14,0]m/s and heading of 90 degrees.

6 Conclusions

In this paper, we have proposed a dynamic UAV path-planning algorithm for tracking a ground target. The algorithm is characterized by a combination of TVFG and LVFG, a point-mass approximation of the target state PDF, and obstacle avoidance strategies. The key advantage of the proposed method is the ability to find the shortest path for a UAV tracking a target, to utilize particle filters for target motion predictions for the case in which road network information is available, and to avoid identified obstacles in the path generations. Theoretic analysis shows that the T+LVFG algorithm outperforms the LVFG alone whenever the tangent lines are available between the UAV's turning limit circle and an objective circle. The

steady-state objective biases of the both T+LVFG and LVFG algorithms are formally derived, as well as the coverage probability calculations. The fact that tangent lines and particle filters are mainly considered to generate path candidates for UAV tracking makes this approach very attractive. The proposed solution methodology can be easily embedded in a mission planning strategy. This dynamic path planning uses fixed-increment time advance, which fits well with any heuristic solution algorithms. Simulation results demonstrate the efficiency and robustness of the new algorithm as a UAV tracks a target in large variety of different experimental scenarios, including different target moving models, winds environments, pre-known road maps and multiple obstacles on the way. Future work will focus on multiple UAVs and multiple target situations.

References

- [1] B. Geiger, and et al, "Optimal Path Planning of UAVs Using Direct Collocation with Nonlinear Programming", AIAA Paper No.2006-6199, AIAA GNC Conference, Aug. 2006.
- [2] S. J. Rasmussen, and at el, "Introduction to the MultiUAV2 Simulation and Its Application to Cooperative Control Research", 2005 American Control Conference, Portland, USA, June 8-10, 2005.
- [3] C. Ferng, and et al, "Distributed Simulation of Forward Reachable Set-Based Control for Multiple Pursuer UAVs", SimTecT 2006.
- [4] R. Wise, "UAV Control and Guidance for Autonomous Cooperative Tracking of a Moving Target", PhD research proposal, University of Washington, 2006.
- [5] M. Winstrand, "Mission Planning and Control of Multiple UAVs", Scientific report, Swedish Defence Research Agency, 1650-1942, October 2004.
- [6] R.H. Stone, and G. Clarke, "Optimization of Transition Maneuvers for a Tail-Sitter Unmanned Air Vehicle (UAV)", Department of Aeronautical Engineering, University of Sydney.
- [7] E. Frew, D. Lawrence and S. Morris, "Coordinated Standoff Tracking of Moving Targets using Lyapunov Guidance Vector Fields", Journal of Guidance, Control, and Dynamics, Vol.31, No.2, March-April 2008.
- [8] H. Chen, KC Chang, and C. S. Agate, "A Dynamic Path Planning Algorithm for UAV Tracking", SPIE 2009.
- [9] G. Collins, and et al, "Cooperative Control of UAVs for Tracking Moving Targets through Information Gain", Phase II STTR Final Report, Toyon Research Corporation, December 28, 2007.
- [10] A. G. Shem, T. A. Mazzuchi and S. Sarkani, "Addressing Uncertainty in UAV Navigation Decision-Making", IEEE Transaction on Aerospace and Electronic Systems, Vol.44, No.1, pp.295-311, January 2008.